The Astrophysical Journal, 845:83 (12pp), 2017 August 10 https://doi.org/10.3847/1538-4357/aa7edd

Formation of Methylamine and Ethylamine in Extraterrestrial Ices and Their Role as Fundamental Building Blocks of Proteinogenic α-amino Acids

Marko Förstel[1,2,3], Alexandre Bergantini[1,2], Pavlo Maksyutenko[1,2,4], Sándor Góbi[1,2], and Ralf I. Kaiser[1,2]
[1] W. M. Keck Research Laboratory in Astrochemistry, University of Hawaii at Manoa, Honolulu, Hawaii, HI, 96822, USA; ralfk@hawaii.edu
[2] Department of Chemistry, University of Hawaii at Manoa, Honolulu, Hawaii, HI, 96822, USA
Received 2017 June 15; revised 2017 July 4; accepted 2017 July 6; published 2017 August 14

Abstract

The –CH–NH_2 moiety represents the fundamental building block of all proteinogenic amino acids, with the cyclic amino acid proline being a special case (–CH–NH– in proline). Exploiting a chemical retrosynthesis, we reveal that methylamine (CH_3NH_2) and/or ethylamine ($CH_3CH_2NH_2$) are essential precursors in the formation of each proteinogenic amino acid. In the present study we elucidate the abiotic formation of methylamine and ethylamine from ammonia (NH_3) and methane (CH_4) ices exposed to secondary electrons generated by energetic cosmic radiation in cometary and interstellar model ices. Our experiments show that methylamine and ethylamine are crucial reaction products in irradiated ices composed of ammonia and methane. Using isotopic substitution studies we further obtain valuable information on the specific reaction pathways toward methylamine. The very recent identification of methylamine and ethylamine together with glycine in the coma of 67P/Churyumov–Gerasimenko underlines their potential to the extraterrestrial formation of amino acids.

Key words: astrochemistry – comets: general – cosmic rays – infrared: ISM – methods: laboratory: molecular – molecular processes

1. Introduction

An understanding of the abiotic formation pathways of extraterrestrial amino acids is still in its infancy although more than 80 amino acids were identified in carbonaceous chondrites (Kvenvolden et al. 1970; Cronin & Pizzarello 1999; Botta et al. 2002; Pizzarello et al. 2004, 2006; Glavin et al. 2006), including the Murchison meteorite and samples returned from comet 81P/Wild 2 by the *Stardust* mission that found glycine to be of extraterrestrial origin (Sandford et al. 2006; Elsila et al. 2009). Note that a tentative observation of the smallest amino acid glycine (NH_2CH_2COOH) in the Orion Molecular Cloud, with column densities up to 4.37×10^{14} cm^{-2}, was initially reported (Kuan et al. 2003), but later disputed (Snyder et al. 2005). Multiple laboratory-based experiments revealed that amino acids can form in energetically processed ice. For example, of the 21 proteinogenic amino acids, glycine, alanine, valine, proline, serine, and aspartic acid were found via gas chromatography–mass spectrometry (GC-MS) in the residues of interstellar ice analogs processed with broadband ultraviolet (UV) radiation (Bernstein et al. 2002; Munoz Caro et al. 2002); electron irradiation of interstellar analog ices produced glycine (Holtom et al. 2005). In Holtom et al. (2005), possible formation pathways toward glycine were discussed. The authors concluded that the synthesis commences with the decomposition of methylamine (CH_3NH_2) to CH_3NH and/or CH_2NH_2 radicals along with suprathermal hydrogen atoms. The latter reacted via the addition of carbon dioxide (CO_2) to the hydroxycarbonyl radical (HOCO). Both radicals can then react to form glycine, a process supported theoretically as well (Woon 2002). Furthermore, possible formation pathways of glycine and serine were discussed in a fluorescence detection liquid chromatography mass spectrometric study of ices that were broadband-photolyzed during the ice deposition (Elsila et al. 2007). Elsila et al. (2007) concluded that neither the Strecker-type synthesis suggested by Bernstein et al. (2002), nor the radical–radical mechanism initially suggested by Woon (Woon 2002), which required the presence of hydrogen cyanide (HCN), could adequately explain the formation of amino acids in their experiment. Alternatively, in an article that studied the formation of dipeptides from irradiated ices, Kaiser et al. discussed two pathways toward amino acids. The first one is the previously described reaction of the CH_2NH_2 radical with the HOCO radical. Alternatively, the authors proposed a formation via acetic acid (CH_3COOH) and ammonia (NH_3) (Kaiser et al. 2013). Acetic acid was previously shown to form in the presence of carbon dioxide (CO_2) and methane (CH_4) (Kim & Kaiser 2010).

A detailed inspection of the molecular structures of the proteinogenic amino acids reveals that the –CH–NH_2 moiety represents a fundamental building block of all amino acids (Figure 1). The only exception is the cyclic proline molecule, where a –CH–NH– group exists. This finding leads to the conclusion that simple molecules that contain the –CH–NH_2 moiety likely represent molecular precursors to the corresponding amino acids. The obvious candidates for these molecules are, for example, the three simplest members of the amines: methylamine (CH_3NH_2), ethylamine ($C_2H_5NH_2$), and propylamine-1 ($C_3H_7NH_2$). A complete retrosynthesis of all amino acids exposed that these amines represent fundamental precursors in the formation of each proteinogenic α-amino acid. This procedure is revealed for six amino acids in Figure 1 and for the remaining amino acids shown in Figures 6–8. A summary of the results is given in Table 3. This finding is fascinating considering that methylamine and ethylamine were observed in extraterrestrial environments. Here, methylamine was detected toward Sgr B2 and Ori A (Fourikis et al. 1974; Kaifu et al. 1974, 1975). A more recent study validated molecular abundances of methylamine toward the Sgr B2(N) molecular core in the order of 10^{-7} relative to molecular hydrogen (Nummelin et al. 2000; Turner 1991).

[3] Present address: Berlin Institute of Technology, IOAP, Hardenbergstrasse 36, 10623 Berlin, Germany.
[4] Present address: Harvard-Smithsonian Center for Astrophysics, 60 Garden Street, Cambridge, MA, 02138, USA.

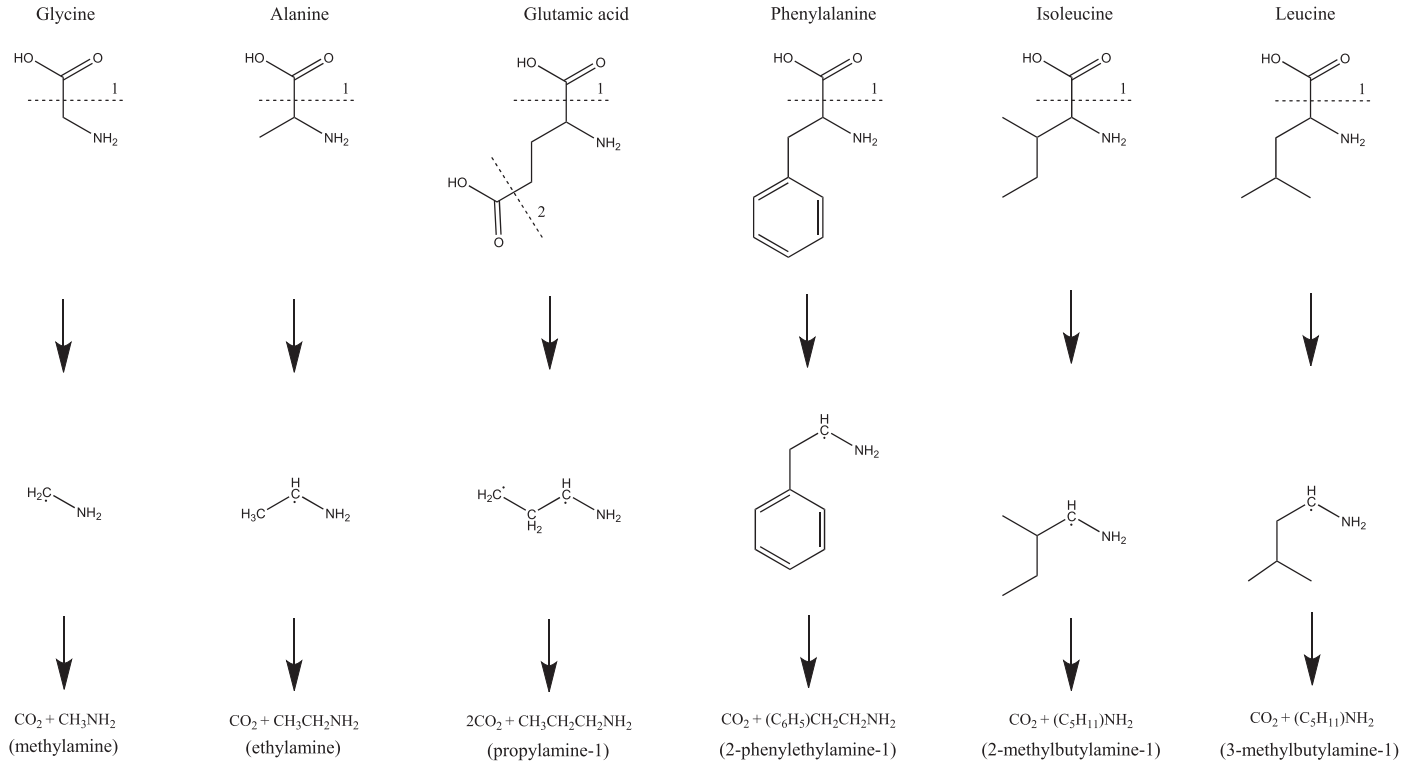

Figure 1. Retrosynthesis of selected amino acids leading to distinct amine precursors. The initial step is generally a separation of the carboxyl group, eventually leading to carbon dioxide (CO_2). Each proteinogenic amino acid can be formed from an amine precursor (see the Appendix, Figures 6–8 and Table 3).

Furthermore, the *Stardust* mission detected methylamine and ethylamine (Glavin et al. 2008). Since these samples contain amino acids as well, the existence of methylamine and ethylamine is expected if they represent precursors of the amino acids. This is amplified by the fact that, very recently, both methylamine and ethylamine were observed on the comet 67P/Churyumov–Gerasimenko (Goesmann et al. 2015).

The gas-phase synthesis and formation in interstellar ices of amines are discussed in the literature. Proposed gas-phase reactions toward methylamine include (unstudied) ion-molecule reactions and dissociative recombination (Leung et al. 1984; Herbst 1985; Maeda & Ohno 2006), or photolysis in gas mixtures containing methane (CH_4) and ammonia (NH_3) (Ogura et al. 1988, 1989). Gardner and McNesby revealed that methylamine forms on icy grains by ionizing radiation (Gardner & McNesby 1980). In a theoretical paper, Woon discussed the formation of methylamine as sequential hydrogenation of hydrogen cyanide (HCN) (Woon 2002). This sequential hydrogenation was experimentally observed in low-temperature ice of hydrogen cyanide that was irradiated with atomic hydrogen (Theulé et al. 2011). Electron irradiation of an ice analog composed of ammonia and methane led to the formation of the cyanide anion (CN^-) (Kim & Kaiser 2011). Kim & Kaiser also showed that, based on the kinetic fits of the temporal evolution of the newly formed molecules, methylamine is a likely precursor in the formation of the cyanide anion. Garrod et al. suggested solely a gas-grain warm-up model where methylamine forms by recombination of the methyl radical (CH_3) and the amidogen radical (NH_2), which are initially formed in the ice from a dissociation of molecular ammonia and methane due to galactic cosmic radiation (Garrod et al. 2008).

In this article, we set out to explore possible formation mechanisms of methylamine and ethylamine representing precursors to amino acids. We exploit a recently established new experimental technique, which allows us to detect the subliming molecules with unprecedented sensitivity: a reflectron time-of-flight mass spectrometer (PI-ReTOF-MS) is coupled with a vacuum ultraviolet ionization source (Jones & Kaiser 2013; Kaiser et al. 2014; Maity et al. 2014). Using photon energies close to the ionization threshold of the molecules, ions are generally detected without fragmentation; in strong contrast to traditional electron impact ionization, this method also allows us to identify structural isomers—molecules with the same chemical formulae but different connectivities of atoms—by selectively tuning the photoionization energy. In combination with isotopic labeling of the parent molecules we can use our detection scheme to obtain detailed insights into the formation mechanism of the generated molecules.

2. Experimental

The experiments were carried out at the W.M. Keck Research Laboratory in Astrochemistry (Jones & Kaiser 2013; Kaiser et al. 2014; Maity et al. 2014; Abplanalp et al. 2016a). A rhodium-coated silver waver mounted on a cold finger is cooled down to 5.5 ± 0.1 K in an ultrahigh vacuum chamber operated at a base pressure of $(2.1 \pm 0.2) \times 10^{-10}$ torr. A premixed 4:1 mixture of ammonia (NH_3, Matheson TriGas, 99.99 %) and methane (CH_4, Advanced Specialty Gases, 99.999%) was deposited onto the waver. The mixture was let into the vacuum chamber through a glass capillary array. The pressure in the chamber increased during the deposition to $(2 \pm 1) \times 10^{-8}$ torr. The deposition was stopped when the ice

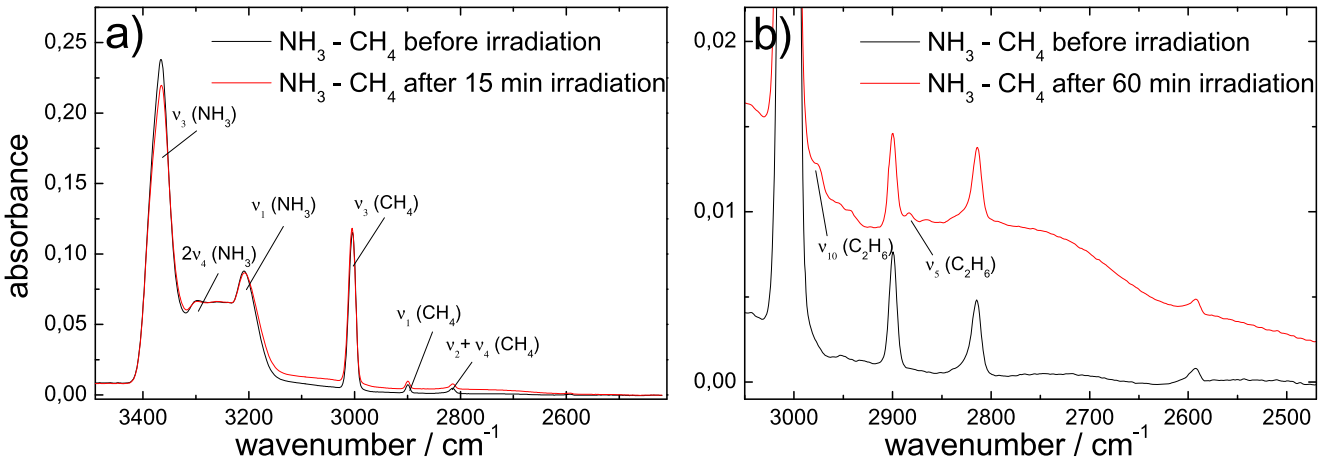

Figure 2. FTIR spectra before (black) and after (red) irradiation of the NH_3/CH_4 ices. (a) No new features are observed after irradiation, besides a broad, unstructured increase in absorbance in the range from 3200 to 2600 cm^{-1}. (b) The emergence of a broad, unstructured band in the 3200–2600 cm^{-1} wavenumber region is observed. Additionally, two small peaks emerged.

thickness reached (600 ± 50) nm. The thickness was monitored in situ using He–Ne laser (CVI Melles-Griot, 25-LHP-213) interferometry at 632.8 nm. During and after the deposition, FTIR spectra (Nicolet 6700, MCT-A) of the ices were recorded in a range of 6000–600 cm^{-1}, with a 4 cm^{-1} resolution. Using known column densities of ammonia (1.1×10^{-17} cm molecule $^{-1}$ at 3366 cm^{-1} (d'Hendecourt & Allamandola 1986)) and methane (1.4×10^{-17} cm molecule $^{-1}$ at 3004 cm^{-1} (Gerakines & Hudson 2015)), we determine the ratio of the molecules in the deposited ices to be (3 ± 1:1) of ammonia to methane. After the deposition, each ice mixture was kept at 5.5 K for 1 hour before it was irradiated with 5 keV electrons at a current of 15 nA for 15 min. Electrons are exploited to simulate the interaction of the ice with galactic cosmic rays (GCRs). GCRs consist mainly of protons with kinetic energies up to PeV. The energy loss of GCRs is predominantly due to ionization of molecules and thus the generation of secondary electrons. These electrons can further ionize molecules, generating electron cascades with typical kinetic energies of a few eV up to some keV (Bennett et al. 2006; Johnson 2012; Abplanalp et al. 2016a, 2016b). The exploited electrons therefore mimic secondary radiation caused by GCRs. Using the Monte Carlo simulation program CASINO (Drouin et al. 2007), we determined the average electron penetration depth to be 290 ± 50 nm, and the fraction of transmitted and backscattered electrons to be 0.05 ± 0.02 and 0.3 ± 0.1, respectively. This results in simulated average doses per irradiated ammonia molecule of about 0.4 ± 0.1 eV and doses per irradiated methane molecule of about 0.4 ± 0.1 eV. After the irradiation, we kept the ice at 5.5 K for 1 hour before the ices were heated with a rate of 0.5 K min^{-1} (temperature programmed desorption, TPD) to 300 K. Molecules that sublimed into the gas phase were ionized with the frequency-tripled third harmonic output of a Nd:YAG laser (Spectra Physics, PRO-250-30) at a wavelength of 10.49 eV and a repetition rate of 30 Hz, and then detected using a reflectron time-of-flight mass spectrometer (ReTOF, Jordan TOF products, Inc.). For time-to-mass conversion, a calibration curve generated by measuring the times-of-flight of a set of ions with known masses (Jones & Kaiser 2013; Kaiser et al. 2014; Maity et al. 2014) was utilized. The same experiment was repeated once without electron irradiation (blank), with a 4:1 mixture of D3-ammonia (ND_3, Sigma Aldrich; 99+% D) and methane (CH_4), and with a 4:1 mixture of ammonia (NH_3) and D4-methane (Sigma Aldrich ; 99+% D). Finally, we carried out experiments with the initial 4:1 NH_3:CH_4 mixture, exploiting two different ionization energies of 9.5 and 8.6 eV.

The 8.6 eV light was generated by resonant four-wave mixing in xenon gas via difference-mixing $\omega_3 = 2\omega_1 - \omega_2$. The third harmonic output of a Nd:YAG laser (Spectra Physics, PRO-270-30) was used to pump a dye laser (Syrah) using Coumarine450 in ethanol to produce light with a wavelength of 445.13 nm, which was then frequency-doubled using a BBO crystal to obtain light with a wavelength of 222.56 nm (ω_1). A second dye laser (Syrah) using Coumarine450 in ethanol pumped by the third harmonic of a second Nd:YAG laser (Spectra Physics, PRO-250-30) was used to produce light with a wavelength of 495 nm (ω_2). The resulting flux was determined to be $(2 \pm 1) \times 10^{10}$ photons per pulse. The 9.5 eV radiation was generated by resonant four-wave mixing in krypton gas. The second harmonic of a Nd:YAG laser was used to pump a dye laser using a mixture of Rhodamine610 and Rhodamine650 in ethanol to produce light with a wavelength of 606.95 nm. This was then frequency-tripled to obtain $\omega_1$with a wavelength of 202.3 nm. ω_2 had a wavelength of 449.8 nm and was generated by pumping a dye laser using Coumarine450 in ethanol with the third harmonic of a Nd:YAG laser. The resulting flux was measured to be $(3 \pm 1) \times 10^{10}$ photons per pulse, i.e., $(0.9 \pm 0.3) \times 10^{12}$ photons s^{-1}.

3. Experimental Results—Infrared Spectra

The FTIR spectra of the NH_3–CH_4 ice before and after irradiation are shown in Figure 2. The unirradiated ice (black trace) depicts a broad feature in the 3450–3100 cm^{-1} region, which exhibits two peaks at 3366 and 3210 cm^{-1}. Additionally, three narrower peaks are observed at 3005, 2899, and 2816 cm^{-1}. The FTIR spectra of the irradiated ice are shown as red traces. Panel (a) shows the result after an irradiation time of 15 minutes. A small, unstructured increase in absorption is observed in a broad range from about 3200 to 2600 cm^{-1}, and a small decrease in the 3366 cm^{-1} feature is noticed as well. No other changes can be found. Panel (b) shows a magnification of a selected area of the FTIR spectrum after a 60 minute irradiation. Again, the broad unstructured feature from 3200 to 2600 cm^{-1} is observed. Additionally, two very small additional features at about 2977 and 2881 cm^{-1} emerged.

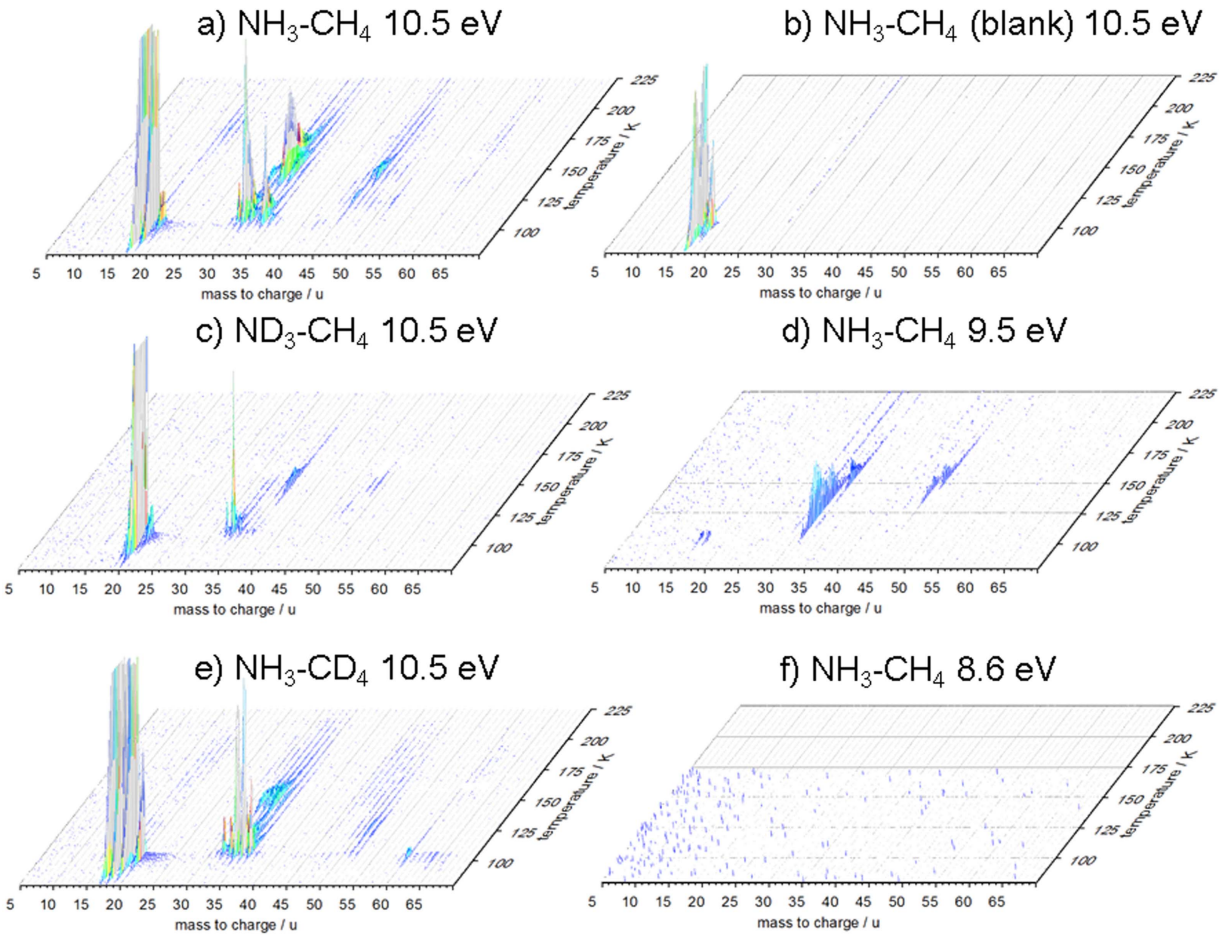

Figure 3. PI-ReTOF-MS spectra obtained at distinct ionization energies of the subliming molecules. Precursor ices and photon energies are indicated in the respective panels. Panel (b) shows the non-irradiated ice (blank). The intensities in panels (a), (c), and (e) are clipped to allow for better representation of the data.

4. Experimental Results—PI-ReTOF-MS Data

The PI-ReTOF-MS TPD results are shown as color-coded maps in Figure 3. Panel (a) depicts the result of the irradiated NH_3–CH_4ice probed with 10.49 eV photons. The strongest signal is observed at a mass-to-charge ratio of 17 (NH_3^+) in a temperature region of 90 to about 110 K. We also observe signals at mass-to-charge ratios of 30, 31, 32, and 33. The strongest signal in this range is observed at a mass-to-charge ratio of 31 (Figure 4). This trace starts to appear at 100 K and has a maximum at 108 K. The second strongest signal in this region is observed at a mass-to-charge ratio of 32. This trace shows a maximum at 150 K. The trace at a mass-to-charge ratio of 30 peaks at 108 K and has two smaller, broader maxima at 125 and 145 K. Furthermore, we observe signals at mass-to-charge ratios of 44, 45, and 46. The trace at a mass-to-charge ratio of 45 has two maxima at 125 and 145 K. The trace at $m/z = 46$ has only one maximum at 145 K. Both traces reveal equal integrated intensity. The trace at a mass-to-charge ratio of 44 depicts the same TPD profile as the trace at a mass-to-charge ratio of 45, although with a factor of about 10 less intensity. A very faint signal is observed at a mass-to-charge ratio of 60.

The TPD profiles of the unirradiated NH_3–CH_4 mixture are shown in panel (b) of Figure 3. Here, we only observe signals at mass-to-charge ratios in the region of 15 to 19, originating from the precursor molecules such as $m/z = 17$ (NH_3^+). The TPD profiles are the same as those observed at these mass-to-charge ratios of the irradiated NH_3–CH_4 mixture (panel a). Panel (c) of Figure 3 depicts the TPD profiles of the irradiated ND_3–CH_4 mixture. The strongest feature is observed here at a mass-to-charge ratio of 20 at a temperature range of 90 to 110 K. Additional features are monitored at mass-to-charge ratios of 32–36 and 45–49. Here, the TPD traces at mass-to-charge ratios of 32–34 peak at 108 K, while the traces at mass-to-charge ratios of 35 and 36 peak at 150 K. The TPD trace at a mass-to-charge ratio of 47 peaks at 125 K and peaks at 145 K at mass-to-charge ratios of 48 and 49.

Panel (e) exhibits the TPD profiles of the irradiated NH_3–CD_4 mixture. The strongest features are observed at mass-to-charge ratios of 17–20 over the temperature range of 90–110 K. Additional features are observed at mass-to-charge ratios of 32–36. The highest intensities are seen at mass-to-charge ratios of 34 and 35, which have about the same intensity, followed by 36 and then 33 and 32. The TPD traces at mass-to-charge ratios of 32 to 35 additionally show intensity in the 140 to 170 K region, peaking at 150 K. Here, the trace at a mass-to-charge ratio of 33 is the strongest, followed by 34, 32, and 35.

Panel (4d) shows the TPD traces of the irradiated NH_3–CH_4 mixture. Here, however, the TPD profiles were obtained using 9.5 eV photons instead of the 10.49 eV as in the previously described panels. The strongest feature observed here is found at a mass-to-charge ratio of 31 in a temperature range of about 100–140 K. A second feature is observed at a mass-to-charge

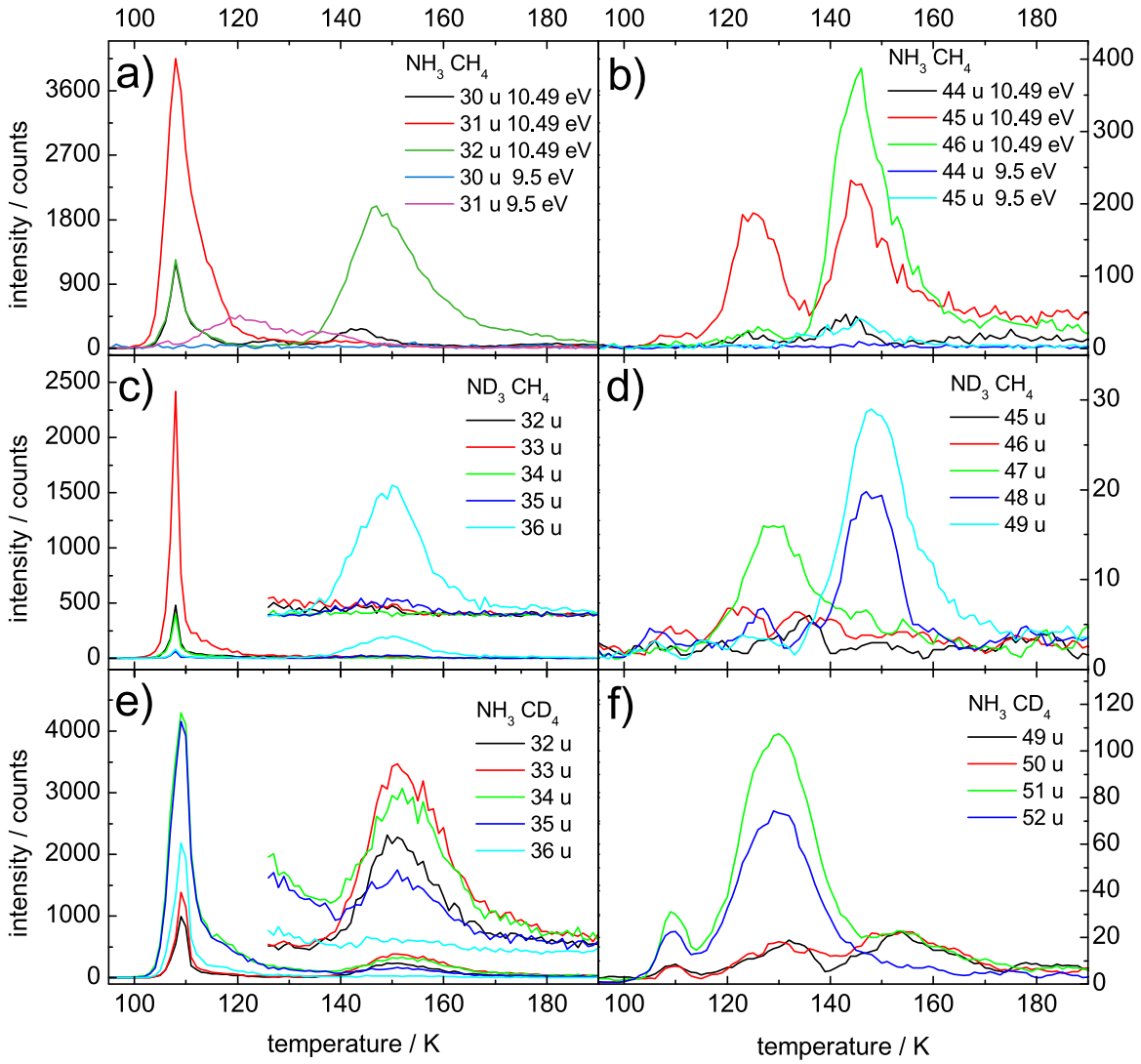

Figure 4. Selected TPD traces of the species under discussion. The *m/z* ratio of each trace is given in the legend. Spectra shown in panels (c)–(f) are taken with an ionization energy of 10.49 eV. Selected traces in panels (c) and (e) are scaled with a factor of 10 and shown with an offset on top of the unscaled spectra.

ratio of 32 in a temperature range of 140–170 K, peaking at 150 K. Some intensity is seen at mass-to-charge ratios of 45 and 46. The TPD trace at a mass-to-charge ratio of 45 has a maximum at around 145 K and the trace at 46 at 150 K.

Finally, panel (f) shows the TPD signal of the irradiated NH_3–CH_4 mixture measured at 8.6 eV in a range of 75–175 K. We observed no signal at this wavelength.

5. Discussion—Infrared Spectra

The interpretation of the FTIR spectra follows closely that of a previous FTIR-QMS study of the same system (Kim & Kaiser 2011). The assignments of the peaks before and after irradiation are indicated in Figure 2. The features in the 3400–3100 cm^{-1} belong to ammonia (NH_3) (ν_3 at 3369 cm^{-1}, ν_1 at 3207 cm^{-1}, and 2 ν_4 at 3290 cm^{-1}). The other features can be associated with methane (CH_4) vibrations (ν_3 at 3004 cm^{-1}, ν_1 at 2898 cm^{-1}, and $\nu_2 + \nu_4$ at 2815 cm^{-1}). Apart from a broad increase in absorption intensity from about 3200 to 2600 cm^{-1} in the irradiated ices, we observe no difference to the pristine ice. These broad absorptions can be linked to the formation of amines and the amino group (–NH_2) (3000–3400 cm^{-1}), along with aliphatic groups (2800 cm^{-1} to 3300 cm^{-1}). Kim and Kaiser (2011) observed several new features after irradiation of a similar ice mixture, among them ethane (C_2H_6), the cyanide anion (CN^-), and features from unspecified alkanes with –CH_3 and –CH_2– moieties. The present experiment exploited an ammonia-to-methane mixture of 4:1, while Kim and Kaiser (2011) used methane-rich ices with an ammonia-to-methane ratio of 1:50. Also, in the present experiment, the irradiation dose is only 0.4 ± 0.1 eV per molecule, compared to 3.8 ± 0.4 eV per molecule in the previous study, i.e., a factor of 10 difference. This means that the present study produces less radical reactants. To probe for comparability with Kim and Kaiser's study (Kim & Kaiser 2011), we carried out one experiment where we increased our irradiation dose to 1.6 ± 0.4 eV per molecule. The resulting FTIR spectrum (Figure 2) shows two features that we identify as the ν_5 and ν_{10} vibrations of ethane at 2883 and 2977 cm^{-1}, respectively. In summary, our experimental study does confirm the formation of ethane (C_2H_6) and higher hydrocarbons, as well as unspecified amines (RNH_2), thus highlighting the limited information provided by FTIR spectroscopy alone.

Table 1
Species Observed and/or Discussed, along with their Respective Chemical Formula, Mass, Ionization Energy (IE), and Appearance Energy (AE) of the Observed Fragments, as well as the Observed Peak Sublimation Temperature

Discussed Species	Chemical Formula	mass/u	IE/eV	Peak Sublimation/ K	Observed
methane[a]	CH_4	16	12.6	⋯	yes[b]
ammonia[a]	NH_3	19	10.07	100	yes
methylamine	NH_2CH_3	31	8.9	108	yes
diimide	N_2H_2	30	9.6	110	yes
hydrazine	N_2H_4	32	8.1	145	yes
ethane[c]	C_2H_6	30	11.5	⋯	yes[b]
ethylamine	$NH_2CH_2CH_3$	45	8.9	128, (145)	yes
dimethylamine	CH_3NHCH_3	45	8.2	(128, 145)	possible
triazene	N_3H_3	45	9.6	>150	yes
methylhydrazine	CH_3NHNH_2	46	7.7	145	very likely
diaminomethyl	$NH_2CH_2NH_2$	46	?	(145)	possible
unknown	$C_2N_2H_8$	60	?	150	⋯
fragment of ethylamine	CH_4N^+	30	AE = 9.7	128, (145)	yes
fragment of ethylamine	$C_2NH_6^+$	44	AE = 9.55	128, (145)	yes
fragment of methylhydrazine	$CN_2H_5^+$	45	AE = 9.2	(145)	possible
fragment of methylhydrazine	$CN_2H_4^+$	44	AE = 9.4	(145)	possible
fragment of methylhydrazine	$CN_2H_3^+$	43	AE = 9.2	(145)	possible

Notes. Peak sublimation temperatures in parentheses indicate that an assignment is ambiguous; see the text for a discussion.
[a] Starting material.
[b] Methane and ethane were only observed with the FTIR spectrometer in the ice.
[c] Ethane formed in the ice under investigation at higher doses.

6. Discussion—PI-ReTOF-MS Data

Let us now discuss and identify species observed via the PI-ReTOF-MS method. The feature at a mass-to-charge ratio of 17 observed in all the 10.49 eV experiments stems from ammonia (NH_3). Ammonia has an ionization energy of 10.02 eV (Qi et al. 1995) and can thus not be observed in the 9.5 or the 8.5 eV experiment. In the ND_3–CH_4 samples, we observe the peak at a mass-to-charge ratio of 20 (ND_3^+). The irradiated CD_4-NH_3mixture shows signals at mass-to-charge ratios of 17 (NH_3^+), 18 (NDH_2^+/$^{15}NH_3^+$), and 19 ($^{15}NDH_2^+$). With an ionization energy of 12.6 eV (Berkowitz et al. 1987) we cannot observe methane in the PI-ReTOF-MS spectra (Table 1).

Based on the simple composition of the ice of only three different types of atoms (H, N, C), the species observed at mass-to-charge ratios of 30–32 can be easily assigned. The species pertaining to the peak at 108 K of the trace at a mass-to-charge ratio of 30 is diimide (N_2H_2), with an ionization energy of 9.6 eV (Ruscic & Berkowitz 1991). This interpretation is in agreement with previously obtained results on irradiated ammonia ice (Förstel et al. 2015, 2016). The other two peaks of this trace are due to fragments of larger molecules and are discussed in the next paragraph. Ethane (C_2H_6) also has a mass-to-charge ratio of 30, but with an ionization energy of 11.5 eV (Bieri et al. 1977), it cannot be ionized. Also, ethane sublimes at around 70 K (Kim & Kaiser 2011).

The signal at a mass-to-charge ratio of 31 stems from methylamine (CH_3NH_2), with an ionization energy of 8.9 eV (Ave & Bowers 1979). Interestingly, the TPD profile of methylamine measured at 10.49 eV differs from that at 9.5 eV. The onset temperature, which is slight above 100 K, is identical in both experiments. However, the 10.49 eV experiment shows a maximum at 108 K, which is not observed for the 9.5 eV experiment. One could argue that the peak observed in the 10.49 eV trace stems from fragments of higher-mass molecules. The only possibility would be methylhydrazine (NH_2NHCH_3),

Table 2
Relative Intensities of the Methylamine Isotopologues in the Irradiated Ices Normalized to 100 for the Most Intense Peak in Each System

mass/u	Intensity NH_3–CH_4	Intensity ND_3–CH_4	Intensity NH_3–CD_4
31	100	0.7	1
32	0	18	19
33	0	100	25
34	0	16	100
35	0	2.5	94
36	0	2.5	44

which can fragment to NCH_5^+ plus NH upon ionization. However, the appearance energy for this process is 11.3 eV and hence this process is not possible under our experimental conditions (Akopyan & Vilesov 1963). The trace at a mass-to-charge ratio of 32 stems from hydrazine (N_2H_4), which has an ionization energy of 8.1 eV (Meot et al. 1984). The measured TPD profile is in agreement with our previous results (Förstel et al. 2015, 2016).

In a similar way we identify the species at mass-to-charge ratios from 44 to 46. Carriers that pertain the observed intensity at $m/z = 45$ can be the isomers ethylamine ($CH_3CH_2NH_2$) and dimethylamine (CH_3NHCH_3), with their respective ionization energies of 8.9 eV (Ohno et al. 1985) and 8.2 eV (Aue et al. 1980), as well as triazene (N_3H_3), which has an ionization energy of 9.6 eV (Foner & Hudson 1958). As described in the previous section, the trace at a mass-to-charge ratio of 45 shows two maxima. This is an indication that at least two different species are observed. Let us concentrate first on the peak holding a maximum at 125 K. Peaks with a similar TPD profile are also observed at mass-to-charge ratios of 30 and 44 in the NH_3–CH_4ice measured with 10.49 eV. Furthermore, they are present at a mass-to-charge ratio of 47 in the ND_3–CH_4 ice

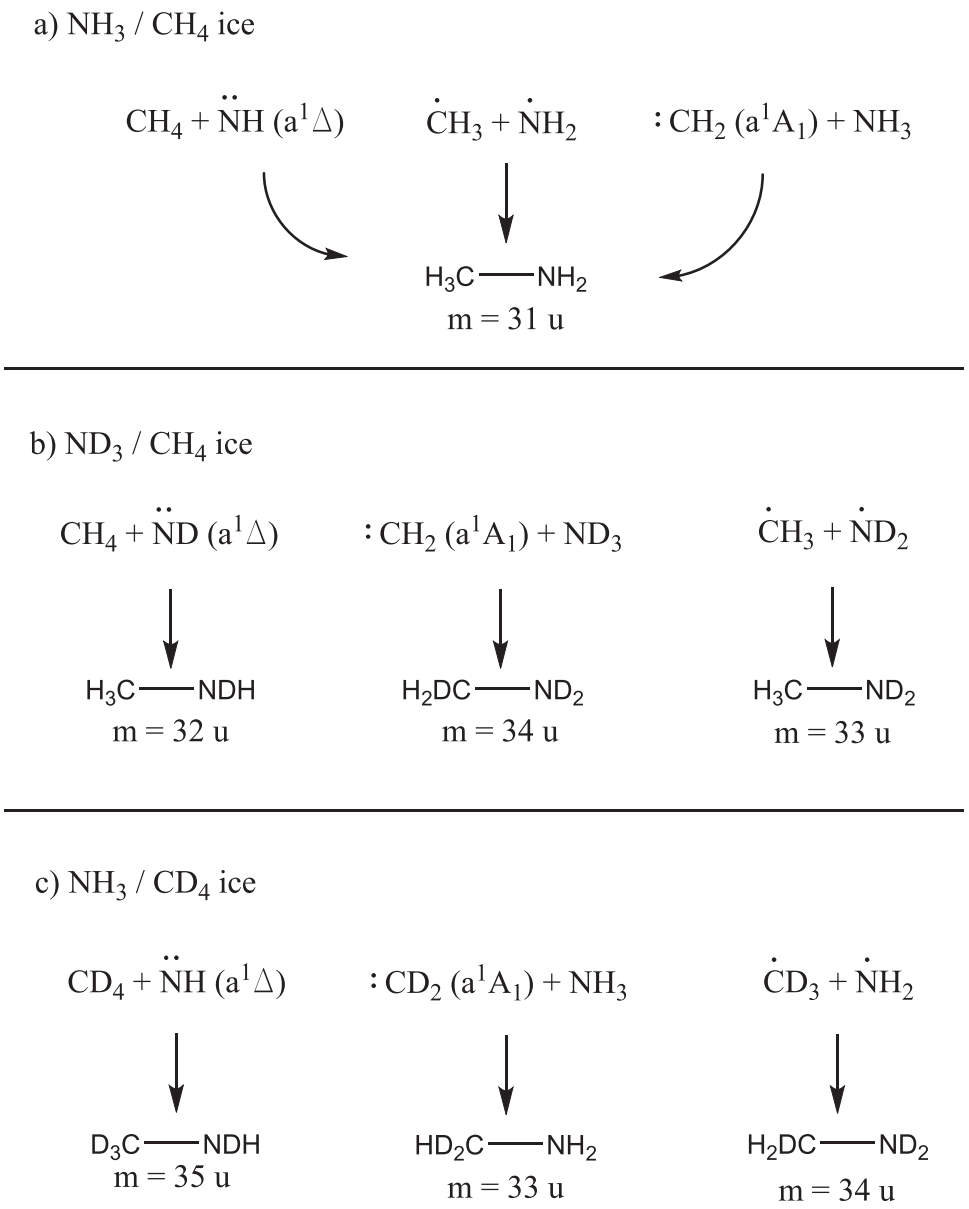

Figure 5. Schematic pathways toward methylamine as discussed in the text, along with the expected mass of the reaction product. Panels (a)–(c) represent the different starting materials of the different ices under consideration.

and at mass-to-charge ratios of 49–52 in the NH_3–CD_4 ice. If the species is ethylamine, we expect that D2-ethylamine ($CH_3CH_2ND_2$), with a mass of 47 u, is formed in the irradiated ND_3–CH_4 mixture and D5-ethylamine ($CD_3CD_2NH_2$) is synthesized with a mass of 50 u in the NH_3–CD_4 mixture. In case of dimethylamine, we would expect predominantly D1-dimethylamine (CH_3–ND–CH_3) with a mass of 46 u in the CH_4–ND_3mixture and D6-dimethylamine (CD_3–NH–CD_3) with a mass of 51 u in the NH_3–CD_4 mixture.

The only peak at 125 K in the ND_3–CH_4 mixture is at a mass-to-charge ratio of 47 and therefore stems most likely from D2-ethylamine ($CH_3CH_2ND_2$). The strongest peak in the NH_3–CD_4 ice at 125 K is at a mass-to-charge ratio of 51, pointing to D6-dimethylamine (CD_3–NH–CD_3). However, this simplified treatment does not consider that upon interaction with ionizing radiation, D and H atoms in closed shell reactants may exchange. Note that ethylamine can fragment upon ionization to $C_2H_6N^+$ (44 u) and CH_4N^+ (30 u), with appearance energies (AE) of 9.55 eV and 9.69 eV, respectively (Lossing et al. 1981). Dimethylamine can also fragment into these fragments; the appearance energies here, however, differ: $C_2H_6N^+$ (AE = 9.4 eV) and CH_4N^+ (AE = 10.8 eV) (Loudon & Webb 1977). Since we observe a small signal at mass-to-charge ratios of 30 in the 10.49 eV probed NH_3–CH_4 ice that matches the TPD profile of the 125 K peak, we conclude that its parent molecule is ethylamine, but not dimethylamine. Summarizing these arguments, we are certain that ethylamine is pertaining to the TPD feature at 125 K.

Let us now concentrate on the peak with a maximum at 145 K of the TPD profile at a mass-to-charge ratio of 45. We can identify several more traces with a similar TPD profile at mass-to-charge ratios 30, 44, and 46 in the irradiated NH_3–CH_4

ice measured at 10.49 eV and at 45 measured at 9.5 eV. Additionally, we observe peaks at mass-to-charge ratios of 48 and 49 in the irradiated ND_3–CH_4 ice and at 49, 50, and 51 in the exposed NH_3–CD_4 ice. In a previous study on neat ammonia ice, we could show that triazene forms and desorbs in a region from 152 to 180 K (Förstel et al. 2016). This means that the higher temperature parts of the second peak can stem from triazene. This is in agreement with the observed peak at a mass-to-charge ratio of 48 in the ND_3–CH_4 ice. The peak at 49 in that ice mixture however, shows that triazene cannot be the only species pertaining to that peak, because triazene can have a maximum of only three deuterium atoms and thus a maximum mass of 48 u.

The traces at mass-to-charge ratios of 44 and 30 point again toward ethylamine as the source for that trace. Another possibility is that some of the intensity of that feature is due to fragmentation of a species with a higher mass. Since the peak at $m/z = 46$ has a similar shape, the species pertaining to that feature is a likely candidate. Possible molecules are methylhydrazine (NH_2NHCH_3), with an ionization energy of 7.7 eV (Meot et al. 1984), and diaminomethane ($NH_2CH_2NH_2$), which, however, is considered to be unstable (DeBons & Loudon 1980). Known fragments of methylhydrazine with AEs below 10.49 eV are $CH_5N_2^+$ (AE = 9.2 eV), $CH_4N_2^+$ (AE = 9.4 eV), $CH_3N_2^+$ (AE = 9.2 eV), and $N_2H_3^+$ (AE = 9.5 eV) (Akopyan & Vilesov 1963). The traces observed at mass-to-charge ratios of 44 and 45 could therefore stem from methylhydrazine. It cannot be excluded that diaminomethane forms and desorbs into the gas phase and is observed here. The peak at a mass-to-charge ratio of 49 in the CH_3-ND_4 is another indication toward methylhydrazine. Again, we would expect D3-methylhydrazine (ND_2NDCH_3), which has a mass of 49 u. Summarizing, we suggest that the peaks in the TPD profiles with a maximum at 145 K stem very likely from triazene and methylhydrazine, but may also have contributions from dimethylamine and ethylamine. We cannot rule out that diaminomethane also contributes to some of the observed intensity.

The small signal at a mass-to-charge ratio of 60 in the NH_3–CH_4 ice and at 61 and 62 in the NH_3–CD_4 irradiated ice shows that some higher-mass species than those described in the previous paragraphs form and desorb. Possible species are ethylenediamine ($NH_2CHCHNH_2$, IE = 8.6 eV) (Kimura et al. 1981), ethylhydrazine ($CH_3CH_2NHNH_2$, IE = 8.1 eV) (Vovna et al. 1975), 1,2-dimethylhydrazine ($CH_3NHNHCH_3$, IE = 8.2 eV), and 1,1-dimethylhydrazine ($(CH_3NCH_3)NH_2$, IE = 8.2 eV) (Bodor et al. 1970). Due to the low observed intensity we cannot distinguish between any of these species. Table 1 summarizes the findings discussed in the previous paragraphs.

7. Discussion—Formation Pathways

Having established the nature of how the amines formed, we are attempting now to draw conclusions on the possible formation pathways. Since the formation pathways of diimide (N_2H_2), hydrazine (N_2H_4), and triazene (N_3H_5) were studied previously (Förstel et al. 2015, 2016), these conclusions are not repeated here, and this discussion focuses on the synthetic routes to amines, especially for the main reaction product: methylamine (CH_3NH_2). Previous studies in our group revealed that upon interaction with ionizing radiation, methane (CH_4) can fragment via simple bond rupture, leading to a methyl radical (CH_3) plus atomic hydrogen (reaction (1)); alternatively, carbene (CH_2) can be formed along with molecular hydrogen or two hydrogen atoms, respectively (reaction (2)). These processes are endoergic by 439, 461, and 897 kJmol^{-1}. Likewise, ammonia (NH_3) can undergo a simple bond rupture process to azanyl (NH_2) plus atomic hydrogen (reaction (3)); likewise, nitrene (NH) can be synthesized together with molecular hydrogen and or hydrogen atoms, respectively (reaction (4)). Once again, these processes are highly endoergic by 454, 423, and 859 kJmol^{-1}, with the required energy supplied by the impinging electrons

$$CH_4 \rightarrow CH_3 + H, \quad (1)$$

$$CH_4 \rightarrow CH_2 + H_2/2H, \quad (2)$$

$$NH_3 \rightarrow NH_2 + H, \quad (3)$$

$$NH_3 \rightarrow NH + H_2/2H. \quad (4)$$

In principle, methyl can recombine with azanyl to form methylamine (CH_3NH_2) (reaction (5)). However, carbene (CH_2) can also insert into an N–H bond of ammonia (reaction (6)), just as nitrene (NH) may insert into a C–H bond of methane and lead to methylamine (CH_3NH_2) (reaction (7)):

$$CH_3 + NH_2 \rightarrow CH_3NH_2, \quad (5)$$

$$CH_2 + NH_3 \rightarrow H\text{–}CH_2\text{–}NH_2, \quad (6)$$

$$NH + CH_4 \rightarrow CH_3\text{–}NH\text{–}H. \quad (7)$$

Which pathway(s) dominate(s)? In the CD_4/NH_3 system, a radical–radical pathway should lead solely to CD_3NH_2 (reaction (8)). On the other hand, the insertion of D2-carbene and nitrene (NH) should follow reactions (9) and (10), respectively:

$$CD_3 + NH_2 \rightarrow CD_3NH_2 (m/z = 34), \quad (8)$$

$$CD_2 + NH_3 \rightarrow H\text{–}CD_2\text{–}NH_2 (m/z = 33), \quad (9)$$

$$NH + CD_4 \rightarrow CD_3\text{–}NH\text{–}D (m/z = 35). \quad (10)$$

Similarly, the CH_4/ND_3 ice should form (partially) deuterated methylamine via radical–radical recombination and/or insertion via reactions (11) to (13):

$$CH_3 + ND_2 \rightarrow CH_3ND_2 (m/z = 33), \quad (11)$$

$$CH_2 + ND_3 \rightarrow D\text{–}CH_2\text{–}ND_2 (m/z = 34), \quad (12)$$

$$ND + CH_4 \rightarrow CH_3\text{–}ND\text{–}H (m/z = 32). \quad (13)$$

Considering the observed mass-to-charge ratios (Table 2) and the fact that only $m/z = 31$ was associated with methylamine formation in the CH_4/NH_3 system, we can conclude that the radical–radical recombinations (reactions (8) and (11)) represent the main contributors to synthesized methylamine. However, our studies reveal that the nitrene (reactions (10) and (13)), as well as carbene insertions (reactions (9) and (12)), also play a role, with nitrene insertions dominating over carbene reactions. This could be the result of the ices being ammonia-rich, thus providing a higher statistical chance that ammonia decomposed to nitrene rather than methane to carbene.

It should be stressed that the overall reaction of methane reacting with ammonia to methylamine is endoergic by 98 kJmol^{-1} (1.0 eV) (reaction (14)) or 534 kJmol^{-1} (5.5 eV) (reaction (15)), respectively:

$$CH_4 + NH_3 \rightarrow CH_3NH_2 + H_2, \quad (14)$$

$$CH_4 + NH_3 \rightarrow CH_3NH_2 + 2H. \quad (15)$$

These energetics alone dictate the necessity of a cosmic-ray-induced non-equilibrium chemistry that leads to the formation of methylamine (CH_3NH_2), with the excess energy being incorporated by the impinging electrons. Note that due to the lower count rates and higher complexity of the ethylamine isotopologues, we cannot provide detailed information on its formation mechanism. However, the aforementioned conclusions suggest that the radical–radical reactions of the ethyl radical (C_2H_5) with the azanyl radical (NH_2) likely lead to ethylamine; nevertheless, nitrene or carbene insertion into a carbon–hydrogen bond of ethane or methylamine are expected to produce ethylamine as well, but with lower probability.

It is important to address one remaining question: are the amines formed at 5 K or during the warm-up of the irradiated ices? Here, basic physical chemistry principles can help to elucidate this issue. Both carbene and nitrene—the key reactants for the experimentally observed insertion processes—both hold triplet electronic ground states ($X^3\,B_1$ and $X^3\Sigma^-$), which are lower by 38 and 146 kJmol^{-1} compared to the electronically excited singlet states ($a^1\,A_1$ and $a^1\Delta$). Carbene and nitrene insert solely in their excited singlet states without entrance barriers; reactions of the ground triplet state have barriers of, e.g., 96 and 52 kJmol^{-1}, upon insertion into a carbon–hydrogen bond of methane (Bauschlicher et al. 1976; Wang et al. 1999). Considering a low temperature like 5 K, only barrier-less reactions proceed, and triplet carbene and nitrene cannot form any amines due to their inherent barriers to the reaction. Considering that singlet carbene and singlet nitrene have lifetimes of at most 18 s (Jacox 2014) and 13 s (Rinnenthal & Gericke 1999), respectively, and that the irradiated ice samples were kept at 5 K for 3600 s prior to their warm-up, we can conclude that the observation of the barrier-less insertion products of carbene and nitrene is the consequence of reactions at 5 K, but not during the warm-up phase. During the 3600 s waiting period, singlet carbenes and nitrenes would have relaxed to their triplet ground state, which in turn would prohibit a reaction since the triplet species have significant barriers to insertion, which cannot be overcome under our experimental conditions in the warm-up phase. Consequently, we can conclude that the reactions of singlet carbene and nitrene can be considered as tracers of a non-equilibrium chemistry that leads to methylamine at 5 K. On the other hand, the barrier-less radical–radical pathway between the methyl and the azanyl radicals can operate at 5 K through the recombination of neighboring radicals, and also operate during the warm-up phase since the ice matrix can trap these doublet radical species. Here, we can follow the evolution of the $-NH_2$ fundamentals of the amines spectroscopically (in the infrared) while the sample is annealed and the methylamines sublime. Considering that the infrared absorptions associated with the amines do not increase during the warm-up (which in turn suggest an absence of radical–radical recombination to methylamine during the warm-up phase), but only decreases as the temperature rises (while methylamine simultaneously sublimates to the gas phase and is observed via PI-ReTOF-MS), we can conclude that radical–radical recombination of the methyl and azanyl radical leading to methylamine also operates at 5 K. These findings, together with the discussed pathways, are summarized in Figure 5. The dominance of radical–radical recombination at 5 K during the exposure of low-temperature ices to energetic electrons was also verified recently by Bergantini et al. (2017) while exploring the formation of acetaldehyde (CH_3CHO) and propanal (C_2H_5CHO) along with their enols.

8. Astrophysical Implications

In this study we have elucidated the formation of two key amines in ices of methane and ammonia under the influence of ionizing radiation: methylamine (CH_3NH_2) and ethylamine ($C_2H_5NH_2$). Methylamine was observed in the interstellar medium toward Sgr B2 and Ori A; in our solar system, methylamine and ethylamine were probed within the framework of the *Stardust* mission and also on comet 67P/Churyumov–Gerasimenko. As precursors to proteinogenic amino acids, methylamine and ethylamine can be synthesized in ammonia-bearing ices from ammonia and the respective hydrocarbons (methane, ethane) via simple radical–radical recombination pathways involving an alkyl radical plus the azanyl radical, but also via more exotic carbene and nitrene insertions, as demonstrated via the use of partially deuterated ice mixtures; these insertion processes can be considered tracers of amine formations that occur within ices at 10 K, but not only during the warm-up of the ices as proposed earlier (Garrod et al. 2008). These results are obtained in an ice mixture that serves as a model for more complex, astrophysically relevant ices. With an increasing methane ratio, we expect more complex amines to be formed, including, for example, linear and even branched C3 and C4 moieties that lead to propylamine and butylamine isomers. Once again, the analysis of samples returned from the *Stardust* mission reveals that both methylamine and ethylamine were found together with glycine and possibly other amino acids (Glavin et al. 2008). This is an indication that these simple amines can be precursors of amino acids, as verified in the retrosynthesis conducted in the present investigation. Interestingly, the recent observation of methylamine, ethylamine, and methane on 67P/Churyumov–Gerasimenko contrasts the lack of ammonia (Goesmann et al. 2015). Based on our results, this might be explained by the high reactivity of ammonia and that of the nitrene and the azanyl radical fragments that formed upon interaction of ionizing radiation with hydrocarbons. Therefore, it is expected that ammonia was present on the comet, but it might have been processed to amines via interaction with GCRs.

We acknowledge support from the US National Science Foundation (AST-1505502) to carry out the experiments. The authors thank the W. M. Keck Foundation for financing the experimental setup. M.F. acknowledges funding for a postdoctoral fellowship from the *Deutsche Forschungsgemeinschaft* (FO 941/1).

Appendix

Retrosyntheses of the remaining amino acids is shown in Figures 6–8. A summary of the obtained products is given in Table 3.

Table 3
Proteinogenic Amino Acids and Their Potential Amine Precursors Extracted via Retrosynthesis (Cystine and Selenocysteine are Omitted)

Amino Acid	Amine	Hydrocarbon Building Block	Other Building Blocks
Alanine	ethylamine	C2	CO_2
Arginine	butyldiamine-1,4	C4	$2\ CO_2 + 2\ NH_3$
Asparagine	ethylamine	C2	$2\ CO_2 + NH_3$
Aspartic acid	ethylamine	C2	$2\ CO_2$
Cysteine	ethylamine	C2	$CO_2 + S$
Glutamic Acid	propylamine-1	C3	$2\ CO_2$
Glutamine	propylamine-1	C3	$2\ CO_2 + NH_3$
Glycine	methylamine	C1	CO_2
Histidine	butylamine-1	C4	$CO + H_2O + 2\ NH_3 + CO_2$
Isoleucine	2-methylbutylamine-1	C5/C4+C1/C3+C2	CO_2
Leucine	3-methylbutylamine-1	C5/C4+C1/C3+C2	CO_2
Lysine	pentyldiamine-1,5	C5/C4+C1/C3+C2	CO_2
Methionine	ethylamine	C2	$CO_2 + CH_3SH$
Phenylalanine	2-phenylethylamine-1	C6+C2	CO_2
Proline	butylamine-1	C4	CO_2
Serine	ethylamine	C2	$CO_2 + O$
Threonine	propylamine-1	C3	$CO_2 + O$
Tryptophan	2-phenyl-butyldiammine-1,4	C6+C4	CO_2
Tyrosine	2-phenylethylamine-1	C6+C2	$CO_2 + O$
Valine	2-methylpropylamine-1	C4/C3+C1	CO_2

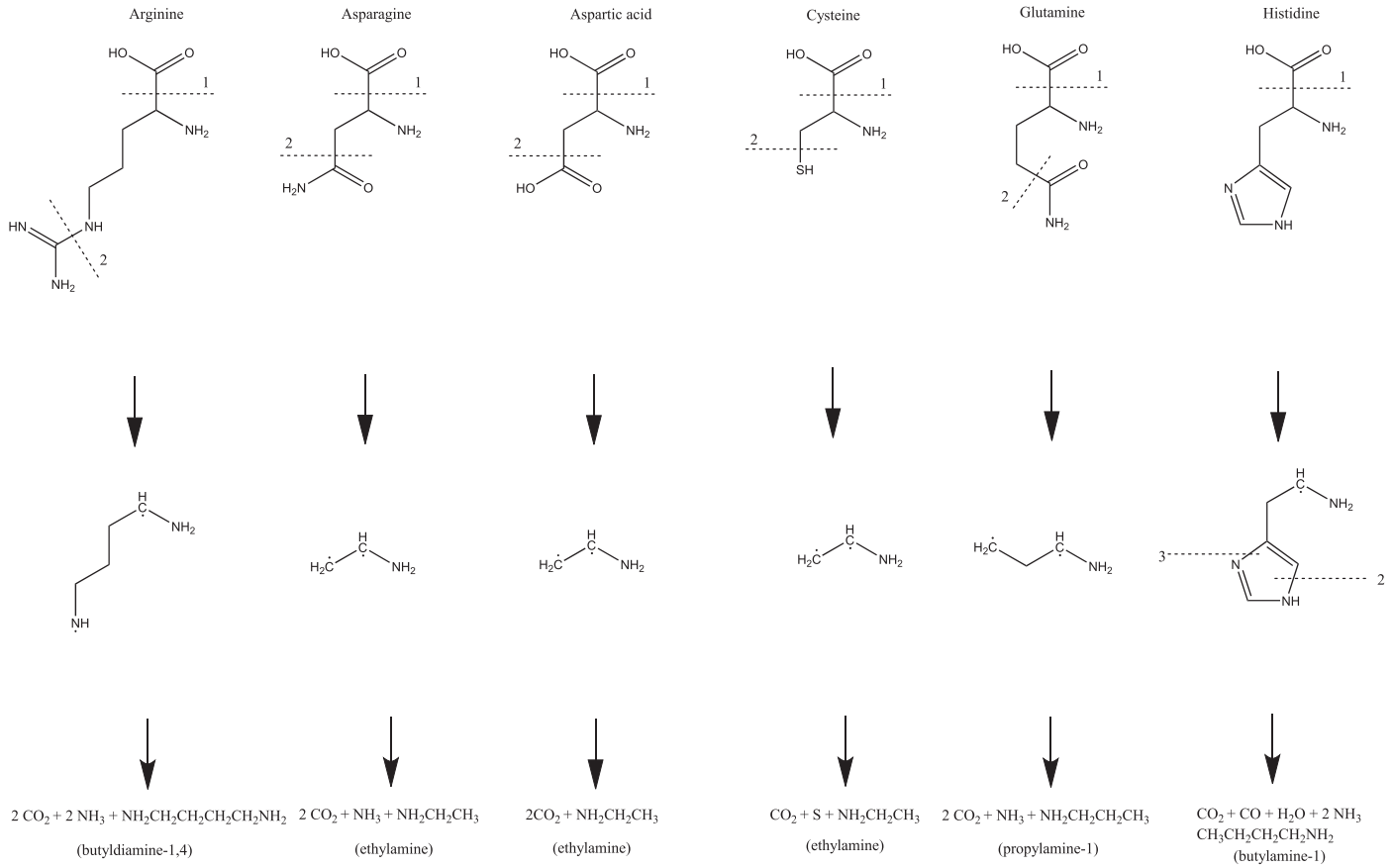

Figure 6. Schematic representation of retrosyntheses of amino acids leading to distinct amines.

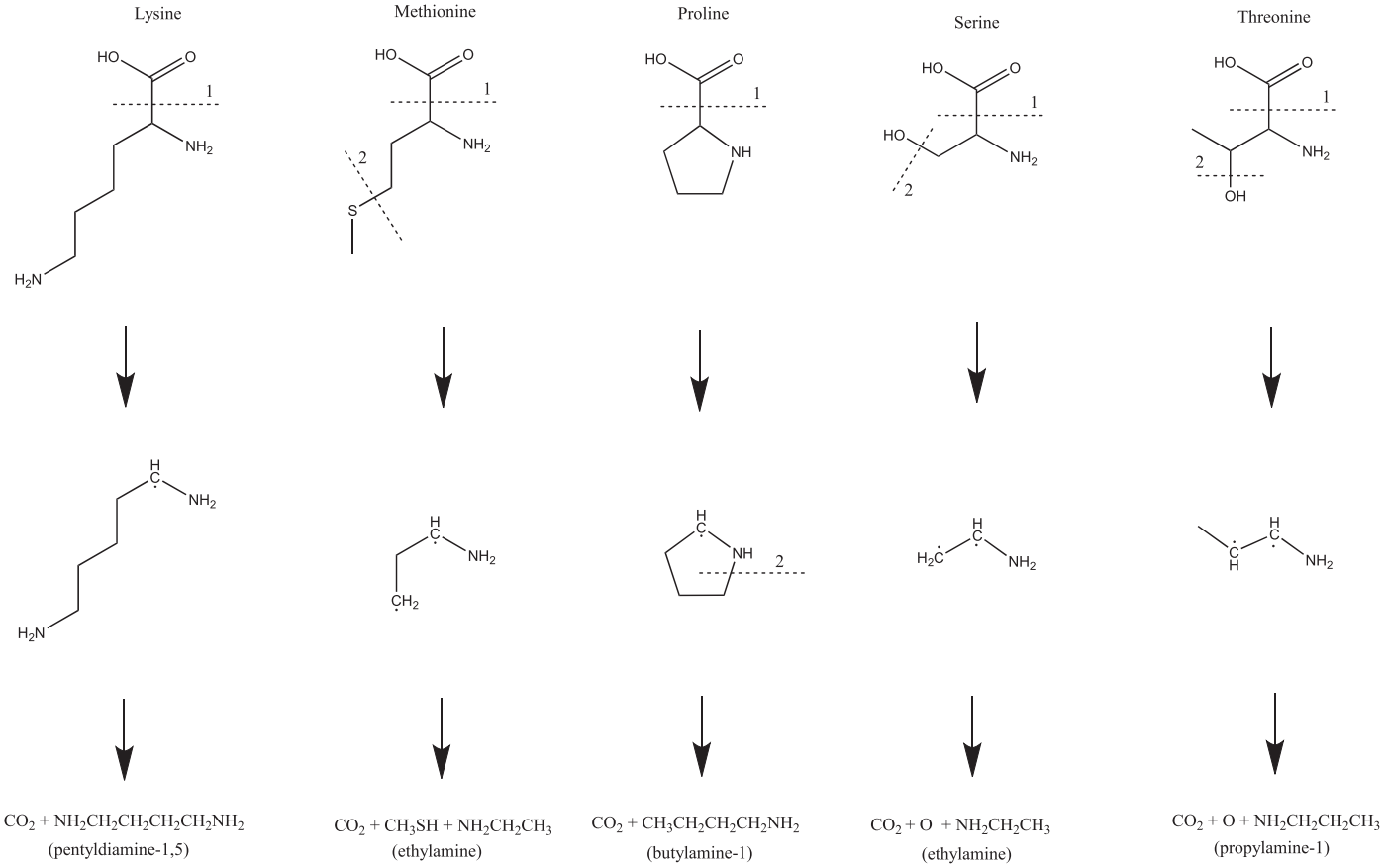

Figure 7. Schematic representation of retrosyntheses of amino acids leading to distinct amines.

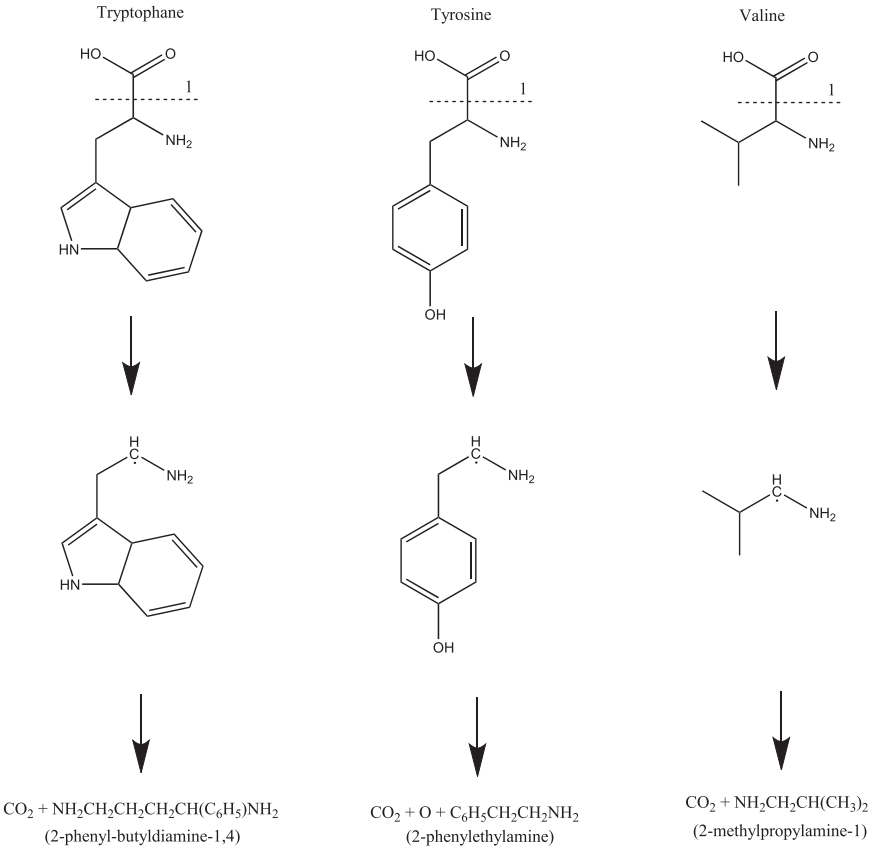

Figure 8. Schematic representation of retrosyntheses of amino acids leading to distinct amines.

ORCID iDs

Marko Förstel https://orcid.org/0000-0002-3630-9494
Alexandre Bergantini https://orcid.org/0000-0003-2279-166X
Ralf I. Kaiser https://orcid.org/0000-0002-7233-7206

References

Abplanalp, M. J., Förstel, M., & Kaiser, R. I. 2016a, CPL, 644, 79
Abplanalp, M. J., Gozem, S., Krylov, A. I., et al. 2016b, PNAS, 113, 7727
Akopyan, M., & Vilesov, F. 1963, Kin. Katal., 4, 32
Aue, D. H., Webb, H. M., Davidson, W. R., et al. 1980, JAChS, 102, 5151
Ave, D. H., & Bowers, M. T. 1979, Gas Phase Ion Chemistry, Vol. 2 (New York: Academy Press)
Bauschlicher, C. W., Jr, Bender, C. F., & Schaefer, H. F., III 1976, JAChS, 98, 3072
Bennett, C. J., Jamieson, C. S., Osumura, Y., & Kaiser, R. I. 2006, ApJ, 653, 792
Bergantini, A., Maksyutenko, P., & Kaiser, R. I. 2017, ApJ, 841, 96
Berkowitz, J., Greene, J., Cho, H., & Ruscić, B. 1987, JChPh, 86, 674
Bernstein, M. P., Dworkin, J. P., Sandford, S. A., Cooper, G. W., & Allamandola, L. J. 2002, Natur, 416, 401
Bieri, G., Burger, F., Heilbronner, E., & Maier, J. P. 1977, Helvetica Chim. Acta, 60, 2213
Bodor, N., Dewar, M., Jennings, W., & Worley, S. 1970, Tetrahedron, 26, 4109
Botta, O., Glavin, D., Kminek, G., & Bada, J. 2002, OLEB, 32, 143
Cronin, J. R., & Pizzarello, S. 1999, AdSpR, 23, 293
DeBons, F. E., & Loudon, G. M. 1980, J. Org. Chem., 45, 1703
d'Hendecourt, L. B., & Allamandola, L. J. 1986, A&AS, 64, 453
Drouin, D., Couture, A. R., Joly, D., et al. 2007, Scanning, 29, 92
Elsila, J. E., Dworkin, J. P., Bernstein, M. P., Martin, M. P., & Sandford, S. A. 2007, ApJ, 660, 911
Elsila, J. E., Glavin, D. P., & Dworkin, J. P. 2009, M&PS, 44, 1323
Foner, S. N., & Hudson, R. L. 1958, JChPh, 29, 442
Förstel, M., Maksyutenko, P., Jones, B. M., et al. 2015, Eur. J. Chem. Phy. & Phy. Chem., 16, 3139
Förstel, M., Tsegaw, Y. A., Maksyutenko, P., et al. 2016, Eur. J. Chem. Phy. & Phy. Chem., 17, 2726
Fourikis, N., Takagi, K., & Morimoto, M. 1974, ApJL, 191, L139
Gardner, E. P., & McNesby, J. R. 1980, J. Photochem., 13, 353
Garrod, R. T., Weaver, S. L. W., & Herbst, E. 2008, ApJ, 682, 283
Gerakines, P. A., & Hudson, R. L. 2015, ApJL, 805, L20
Glavin, D. P., Dworkin, J. P., Aubrey, A., et al. 2006, M&PS, 41, 889
Glavin, D. P., Dworkin, J. P., & Sandford, S. A. 2008, M&PS, 43, 399
Goesmann, F., Rosenbauer, H., Bredehöft, J. H., et al. 2015, Sci, 349, aab0689
Herbst, E. 1985, ApJ, 292, 484
Holtom, P. D., Bennett, C. J., Osamura, Y., Mason, N. J., & Kaiser, R. I. 2005, ApJ, 626, 940
Jacox, M. E. 2014, in NIST Chemistry WebBook, NIST Standard Reference Database Number 69, ed. P. J. Linstrom & W. G. Mallard (Gaithersburg, MD: NIST)
Johnson, R. E. 2012, Energetic Charged-Particle Interactions With Atmospheres and Surfaces (London: Springer)
Jones, B. M., & Kaiser, R. I. 2013, J. Phy. Chem. Letters, 4, 1965
Kaifu, N., Morimoto, M., Nagane, K., et al. 1974, ApJL, 191, L135
Kaifu, N., Takagi, K., & Kojima, T. 1975, ApJL, 198, L85
Kaiser, R. I., Maity, S., & Jones, B. M. 2014, PCCP, 16, 3399
Kaiser, R. I., Stockton, A. M., Kim, Y. S., Jensen, E. C., & Mathies, R. A. 2013, ApJ, 765, 111
Kim, Y. S., & Kaiser, R. I. 2010, ApJ, 725, 1002
Kim, Y. S., & Kaiser, R. I. 2011, ApJ, 729, 68
Kimura, K., Katsumata, S., Achiba, Y., Yamazaki, T., & Iwata, S. 1981, in Handbook of HeI Photoelectron Spectra of Fundamental Organic Molecules (Tokyo: Japan Scientific Society Press), 161
Kuan, Y.-J., Charnley, S. B., Huang, H.-C., Tseng, W.-L., & Kisiel, Z. 2003, ApJ, 593, 848
Kvenvolden, K., Lawless, J., Pering, K., et al. 1970, Natur, 228, 928
Leung, C. M., Herbst, E., & Huebner, W. 1984, ApJS, 56, 231
Lossing, F., Lam, Y.-T., & Maccoll, A. 1981, CaJCh, 59, 2228
Loudon, A., & Webb, K. 1977, J. Org. Mass Spectrom., 12, 283
Maeda, S., & Ohno, K. 2006, ApJ, 640, 823
Maity, S., Kaiser, R. I., & Jones, B. M. 2014, FaDi, 168, 485
Meot-Ner, M., Nelsen, F. N., Willi, M. F., & Frigo, T. B. 1984, JAChS, 106, 7384
Munoz Caro, G. M., Meierhenrich, U. J., Schutte, W. A., et al. 2002, Natur, 416, 403
Nummelin, A., Bergman, P., Hjalmarson, Å., et al. 2000, ApJS, 128, 213
Ogura, K., Migita, C., & Yamada, T. 1989, J. Photochem. & Photobio. A: Chem., 49, 53
Ogura, K., Migita, C. T., & Yamada, T. 1988, Chem. Letters, 17, 1563
Ohno, K., Imai, K., & Harada, Y. 1985, JAChS, 107, 8078
Pizzarello, S., Cooper, G., & Flynn, G. 2006, in Meteorites and the Early Solar System II, Vol. 1, ed. D. S. Lauretta & H. Y. McSween, Jr. (Tucson, AZ: Univ. Arizona Press), 625
Pizzarello, S., Huang, Y., & Fuller, M. 2004, GeCoA, 68, 4963
Qi, F., Sheng, L., Zhang, Y., Yu, S., & Li, W.-K. 1995, ChPhL, 234, 450
Rinnenthal, J. L., & Gericke, K.-H. 1999, JMoSp, 198, 115
Ruscic, B., & Berkowitz, J. 1991, JChPh, 95, 4378
Sandford, S. A., Aléon, J., Alexander, C. MO'D, et al. 2006, Sci, 314, 1720
Snyder, L. E., Lovas, F. J., Hollis, J. M., et al. 2005, ApJ, 619, 914
Theulé, P., Borget, F., Mispelaer, F., et al. 2011, A&A, 534, A64
Turner, B. 1991, ApJS, 76, 617
Vovna, V., Vilesov, F., & Lopatin, S. 1975, OptSp, 38, 143
Wang, B., Hou, H., & Gu, Y. 1999, JPCA, 103, 9049
Woon, D. E. 2002, ApJL, 571, L177